COMPARISON OF PORE SIZE DISTRIBUTION BY NMR RELAXATION AND NMR CRYOPOROMETRY IN SHALES

M. Fleury[1], R. Fabre[1], J.B.W. Webber[2]
[1]IFP Energies nouvelles, 1 avenue de Bois-Préau, 92852 Rueil-Malmaison, France.
[2]Lab-Tools Ltd, Lakesview International Business Park, Hersden, Canterbury, Kent CT3 4JZ, UK

This paper was prepared for presentation at the International Symposium of the Society of Core Analysts held in St. John's Newfoundland and Labrador, Canada, 16-21 August, 2015

ABSTRACT

The characterization of shales is challenging due to their very small pore sizes. In a previous paper, we have shown that Nuclear Magnetic Resonance relaxation techniques are well suited for detecting and quantifying water in nanopores. However, the distribution of relaxation times does not necessarily represent the distribution of pore sizes in the sample due to pore diffusive coupling. Indeed, all pore sizes below the diffusion length will be averaged around a single relaxation time representing an average volume to an average surface ratio. We illustrate the above-mentioned effects by comparing NMR relaxation and cryoporometry data on the same sample. The NMR cryoporometry experiment relies on the shift of the melting temperature of the saturating liquid, which is itself a function of pore size according to Gibbs-Thomson theory. The experiments were performed first on a model system made of a mixture of two calibrated porous glass (15 and 139 nm) and secondly on a shale. On the model system, the cryoporometry results are in quantitative agreement with the expectations but the T_2 distribution is strongly modified by pore coupling and only the 15nm pore size population can be identified. Pore coupling is also clearly identified by T_2-store-T_2 experiments. On the shale sample, the pore size distribution obtained from cryoporometry experiments is quasi uniform from 2 up to 100 nm, while the T_2 distribution is log-normal and relatively narrow. The disagreement between these two results is also explained by pore coupling.

INTRODUCTION

The characterization of shales requires revisiting petrophysical techniques. For example when considering porosity, strong disagreement between standard techniques can result if inappropriate protocols are used [1]. For the pore size distribution, the mercury injection technique may also fail to capture the very small range of pore sizes below ∅ 6nm. Also, the sample drying can interfere with the PICP measurement in the presence of clays. For this point of view, NMR techniques requiring saturated samples are non-disturbing and well suited for pore sizes down to nanometers. For example we have shown that NMR relaxation techniques are adequate for detecting and quantifying water in the interlayer of smectites [2].

For the range of pore size considered, 1nm up to 1µm, other techniques routinely used in the field of catalysis are available. Gas adsorption and thermo-porometry are some examples. NMR cryoporometry is not new [3] but has not been widely used although it has several advantages. In low field systems, it only requires a device to control the temperature of the sample very accurately. Very few results have been published so far about this technique for characterizing shales and we believe it has a great potential.

In this work, we emphasize that standard T_2 distribution cannot always capture the true pore size distribution due to strong pore coupling effects. These effects are ideally demonstrated by comparing NMR cryoporometry and relaxation results on the same sample. For this purpose, we used calibrated porous glasses as a model system, and a shale sample from a tight clayey formation.

BACKGROUND: NMR CRYOPOROMETRY

NMR cryoporometry is based on the shift of the freezing or melting point of the fluid saturating the porous media according to:

$$\Delta T_m(x) = -\frac{k_{GT}}{x} \quad (1)$$

where k_{GT} is the so-called Gibbs-Thomson constant and x is the pore size. The above equation has been established rigorously in the case of a cylinder, hence x may correspond to the diameter of this cylinder. However, when the shape is undefined, the pore size x will rather correspond to a curvature $\partial V/\partial S$ in the melting cycle [4]. In this work, we only consider the melting cycle to avoid hysteresis problems and to allow a large pore size to be explored given the capabilities of our instrument. If one detects the amount of liquid volume V(T) present in the sample at a function of temperature T, one can obtain the pore size distribution P(x) from the derivative of the V(T) curve using the following equation:

$$P(x) = \frac{dV}{dx} = -\frac{k_{GT}}{x^2}.\frac{dV}{dT} \quad (2)$$

Since pore size distributions are usually plotted using logarithmic scales, it is more useful to plot the following distribution:

$$P^*(x) = \frac{dV}{dln(x)} = -\frac{k_{GT}}{x}.\frac{dV}{dT} \quad (3)$$

in a similar way as in mercury intrusion experiments for example.

The constant k_{GT} actually contains complex and multiple physical phenomena but it has been shown that coherent values are obtained on a series of model materials characterized by other experimental techniques, such as gas adsorption [5]. In this work we will take the value k_{GT}=58.2 K.nm for water. With this value and the range of temperatures available in our instrument, the range of pore sizes that can be explored is about 2 to 600

nm (Figure 1). For the upper value, we assumed that a temperature resolution of 0.1°C is achieved. Due to a 1/x sensitivity, the method has a non-uniform resolution (excellent around 10 nm and potentially very poor around 500nm) if the temperature is increased linearly, as explained later.

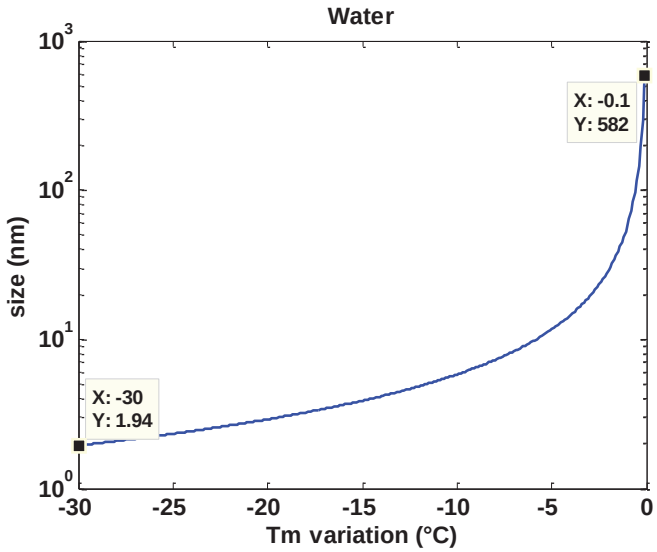

Figure 1: range of pore sizes that can be explored with water considering a variation of the melting temperature Tm from 0 down to -30°C.

A very common interrogation is whether the pore size is modified during the freezing cycle due to the formation of ice with a smaller density. NMR cryoporometry is actually only one branch out of many cryoporometry techniques and freezing-melting cycles are used routinely for example in Differential Scanning Calorimetry (DSC) techniques without any damage to samples. A key aspect is certainly to avoid freezing by nucleation and this can be achieved by surrounding the sample with bulk water and performing a freezing-melting-freezing cycle prior to the main melting cryoporometry experiment, without melting the bulk phase at the second step [4]. Also, the ice formed in pores has a different structure referred as plastic ice [6].

MATERIALS AND NMR METHODS

NMR Relaxation Methods

The experiments have been carried out on a Maran Ultra proton spectrometer from Oxford Instruments with a proton Larmor frequency of 23.7 MHz. Beside standard CPMG measurements, 2D T_2-store-T_2 exchange maps were measured using the methodology presented elsewhere [7].

For the cryoporometry experiments, the liquid volume quantity is measured using a single Hahn echo chosen at an appropriate echo spacing τ to avoid detecting ice. Indeed, although normal ice has a T_2 relaxation time of 8 µs (and T_1=70 s), some of the ice

formed in pores may have different characteristics. The τ value is also selected as a function of the sample in order to maintain an adequate signal to noise ratio. For the calibrated porous glass, τ=500µs, and for the shale, τ=100µs (i.e. the NMR amplitude is taken at 1ms and 0.2ms respectively). Unfortunately, a CPMG sequence in which one would choose any appropriate time cannot be used because the radio-frequency pulses produce a significant and measurable heating of the sample, interfering with the imposed temperature ramps.

NMR Cryoporometry Device

The cryoporometry device (Figure 2) designed by Lab-Tools Ltd is composed of a special probe that can be inserted inside the magnets, replacing standard probes from the manufacturer of the NMR instrument. In this probe, a glass tube of diameter 5mm o.d. can be inserted, and the sample can have a maximum height of about 20 mm. This tube is in close contact with a copper tube connected to a Peltier system for regulating very precisely the temperature. Heat resulting from the cooling of the sample is evacuated from the Peltier system using water circulating at a temperature of 5°C. Temperature is measured using thermocouples constantly calibrated with a reference bath at 0°C. They are placed at two locations : as closed as possible to the sample above the NMR antenna, and close to the Peltier system. With a maximum current of 3A at 12V, the temperature can decrease down to -31°C. A software controlling the power supply allows programming temperature ramps as small as 0.002 °C/min. Such small ramps are only set close to the bulk melting point and non-linear temperature ramps are generally used to speed up experiments (Figure 3). Since a NMR measurement may take 2 minutes and temperatures are also averaged over 2 minutes, the corresponding NMR signal may be averaged over a temperature gradient of 0.004°C. From this principle, a theoretical resolution curve can be calculated as a function of pore size (Figure 3). For example, at 600 nm, the resolution is limited to about ±11nm.

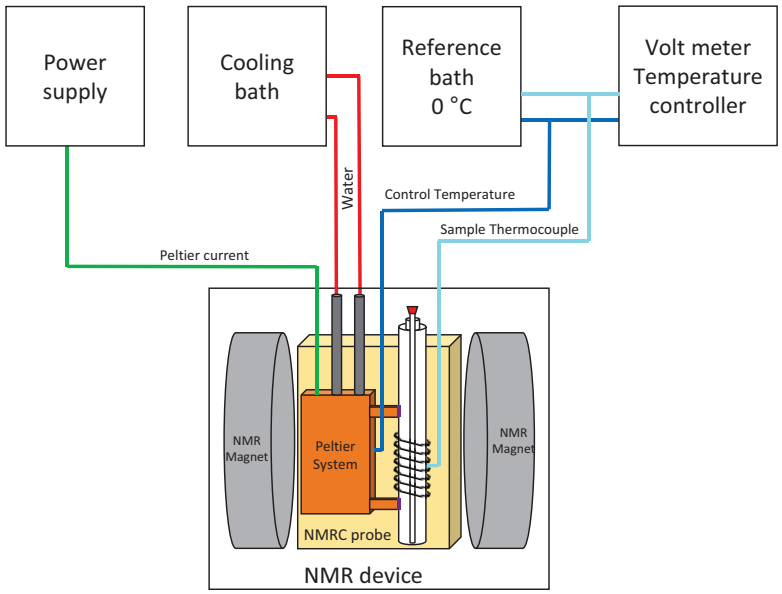

Figure 2: Schematic of the NMR cryoporometry probe and associated control components.

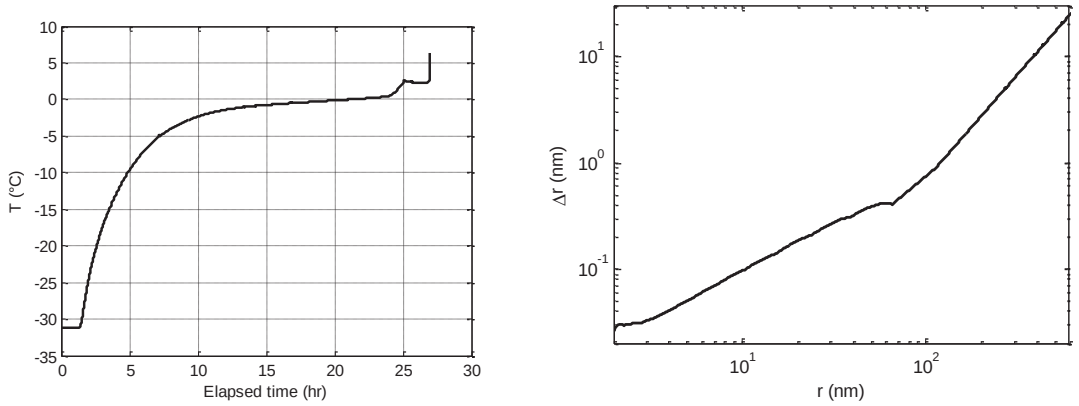

Figure 3: Typical temperature profiles for shale samples (left). Temperature increase is reduced to 0.002°C/min close to the bulk melting point. Theoretical pore size resolution assuming a measuring time of 120 s (right).

Samples

We used a model system composed of calibrated porous glass (CPG from BAM, Federal Institute for Materials Research and Testing, Germany) of mean pore sizes d_{50}=15.1±0.2nm (ERM-FD121, pore volume 624.6mm^3/g) and d_{50}=139±3.7nm (ERM-FD122, pore volume 924.4mm^3/g) as measured by high pressure mercury injection experiments. Taking a glass density of 2.5, the porosity of these medium are 25% and 37% respectively. The shape of the pores in these medium are tubular like. These reference materials are delivered as grains of mean diameter 55µm (ERM-FD121) and

90µm (ERM-FD122). We made a grain pack from these materials by mixing 80.5 mg of ERM-FD121 and 55.0mg of ERM-FD122 in a 5mm tube (Figure 4).

The shale sample originates from the Callovo-Oxfordian (COx) formation at a depth of 604m (EST433 borehole of Montiers-sur Saulx, France). At this depth of the COx formation, a high clayey unit is present with carbonate nodules dispersed in the medium (20%wt) playing a minor role in terms of porosity or permeability [8]. On a plug size, the porosity measured by NMR and water permeability measured by steady-state were respectively 14.8% and 7.3nD. We extracted from the plug a small cylinder of diameter 4mm and length 20mm for the cryoporometry experiments.

RESULTS

We show the results obtained on the above-mentioned samples. For the CPG medium, the objectives are to test the cryoporometry device as well as comparing the measured pore size distributions with NMR relaxation.

Calibrated Porous Glass

The cyoporometry experiments on the CPG mixture gave the expected results (Figure 5); we observe 3 plateaus that correspond to the successive melting of the 15nm CPG, the 139nm CPG and finally the inter-grain phase surrounding the CPG grains. Each plateau value allows calculating the fraction of each phase as detailed later. Then, the curve was fitted with spline functions in order to extract the derivative and obtain the pore size distribution, as detailed in equation 3. The pore sizes obtained fall very close to the values given by the manufacturer using MICP measurements: 14 nm and 147 nm (Figure 6). First, although we compare two measurements with different physical mechanisms, the good agreement comes from the fact that both techniques use a cylinder shape for the pores. Second, the pore size values obtained from cryoporometry depend (i) on the constant k_{GT} that can vary from one author to another, (ii) on the fine adjustment of the bulk melting temperature which is not known very precisely (although thermocouples are calibrated very accurately). The increase of temperature vs. time is a minor source of uncertainty, as shown above. Qualitatively, the narrow width of the 15nm CPG medium is in agreement with the MICP distribution given by the manufacturer (not shown), and the width of the 139nm CPG is larger. Concerning the fraction of each population, cryoporometry results are in good agreement with simple weight measurement of water and CPG materials inserted in the tube (Table 1)

The T_2 distribution measured for the CPG mixture at 30°C is essentially bimodal (Figure 7). At first glance, the peak at T_2~30ms corresponds to the 15nm population, whereas the wider peak centered around T_2~220ms correspond to the 139nm population. However, the inter-grain water is not identified and the tail at T_2>1s correspond in fact to a small amount of supernatant water at the top of the CPG grain pack in the tube (it was later removed for performing the T_2-store-T_2 exchange experiments). Given the weak surface relaxivity of this clean material (~0.25 µm/s), the inter-granular water is expected close

the bulk value. In fact, the T_2 distribution is strongly influenced by pore coupling, i.e. molecules are diffusing in and out of the porous glass and exchange with inter-granular water. Hence, none of the peaks are representative of the different population fractions. A strong evidence is given by the T_2-store-T_2 map (Figure 8) measured separately at a temperature of 30°C. On such map, pore coupling is unambiguously indicated by the presence of off-diagonal peaks located symmetrically on both sides. The exchange time was chosen here at 300ms but other smaller values give similar (but weaker) off-diagonal peaks. However, the details of the exchanges cannot be known precisely. Taking a diffusion coefficient of water of 0.5x 10^{-9} m^2/s, the diffusion length at 300ms is about 30µm. Therefore, inter-granular water can partially exchange with the porous grains for each size. Most probably, exchanges between grains are also possible. Further evidence is given by the T_2 distribution measured at -0.15°C (Figure 5) when the inter-granular water is frozen but the 15nm and 139nm CPG are melted (Figure 9). We obtain in this case two narrow peaks that are truly representative of the relaxation time and fraction of each population. Focusing at the fraction of each population (Table 1), we retrieve the appropriate values measured by cryoporometry and weight.

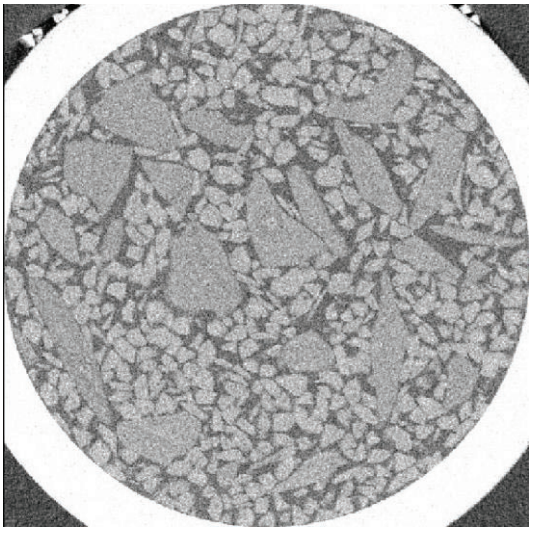

Figure 4: Micro-CT image of the CPG mixture. The diameter is 4 mm. Small grains: 15 nm, large grains: 139nm

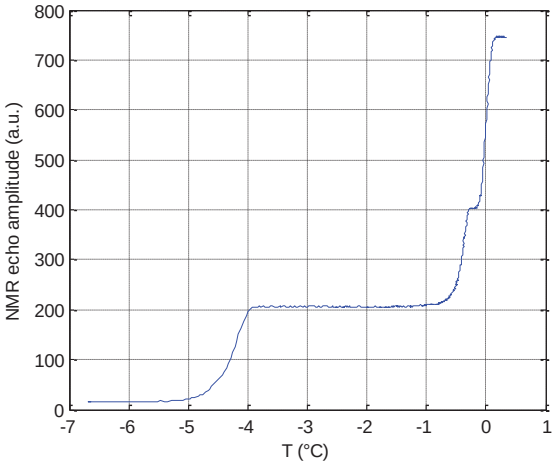

Figure 5: Hahn echo amplitude at 1ms as a function of temperature. The 3 plateaus correspond to the successive melting of the 15nm CPG, the 139nm CPG and finally the bulk phase surrounding the CPG grains around 0°C.

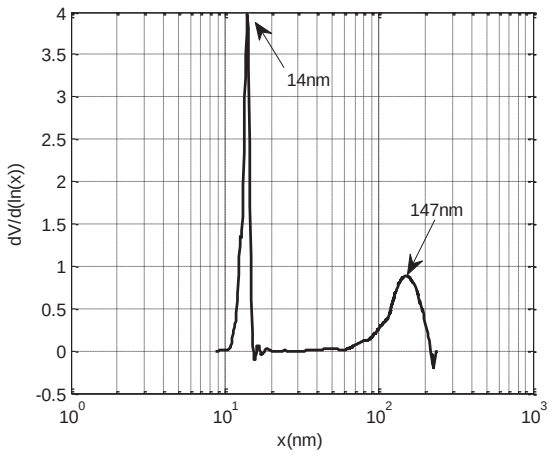

Figure 6: Pore size distribution on the CPG mixture obtained from the cryoporometry experiment (raw data shown in Figure 5).

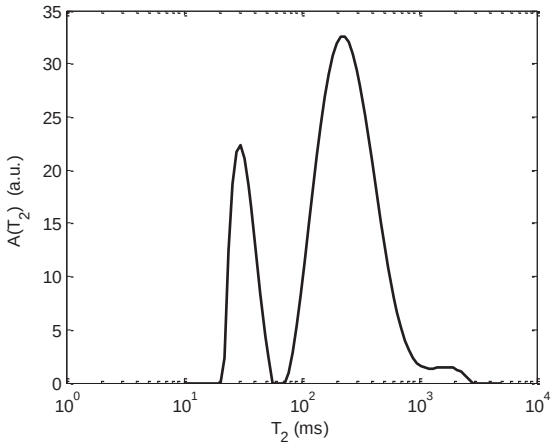

Figure 7: T_2 distribution of the CPG mixture at 30°C.

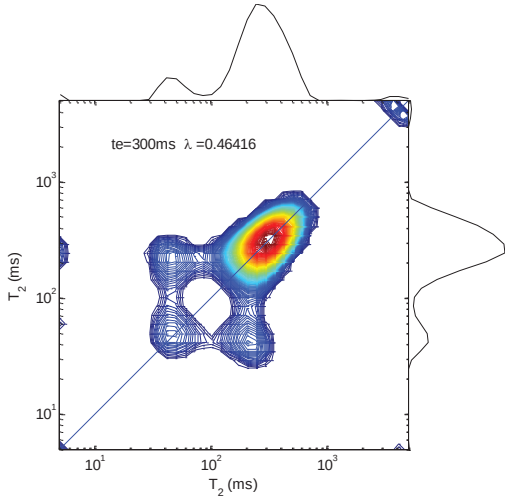

Figure 8: T_2-store-T_2 exchange experiment t 30°C on the CPG mixture performed at an exchange time te=300 ms.

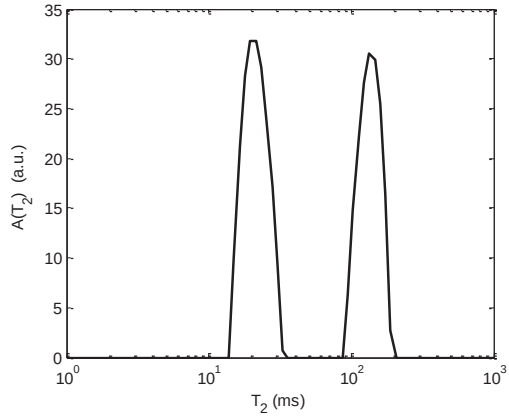

Figure 9: T_2 distribution obtained when the inter-grain water is frozen at -0.15°C, inhibiting diffusive exchange. The two narrow peaks are located at T_2=20ms and 138ms.

Shale Sample

The cryoporometry experiment was performed on the shale sample using the largest possible range of temperature (-31°C). The measured pore size distribution (Figure 10) is relatively uniform from 2 up to 100nm, in qualitative agreement with results obtained on a Barnett shale [9]. Due to the low permeability of this sample (7 nD), pore sizes larger than 100nm are not expected. As opposed to this large distribution, the T_2 distribution

(Figure 11) has a more classical shape close to log-normal (note here that no shape is imposed in the data processing). Compared to the model system, the T_2 values are much shorter due to a larger surface relaxivity (typically of the order of 5 µm/s) but also due to a much larger surface to volume ratio generated by pore size as small as 2 nm. The strong disagreement with cryoporometry results can be explained by pore coupling as discussed further later. We also measured the T_2 distribution at several temperature (but in a separate experiment) and found that the distribution is simply shifting as the temperature is increasing and the largest pore sizes gradually melting. The small pores are not described by the tail at small values inside the T_2 distribution at full saturation.

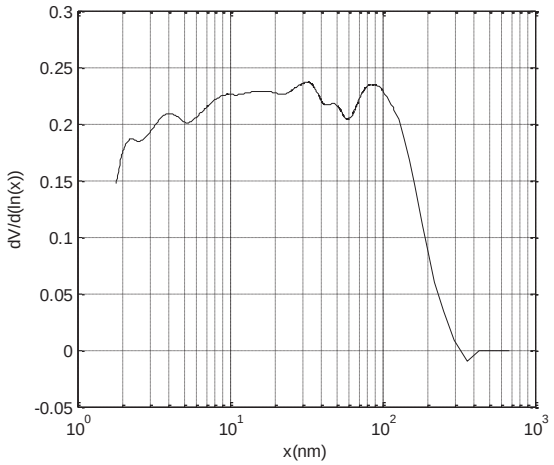

Figure 10: Pore size distribution obtained on the shale sample, cryoporometry technique.

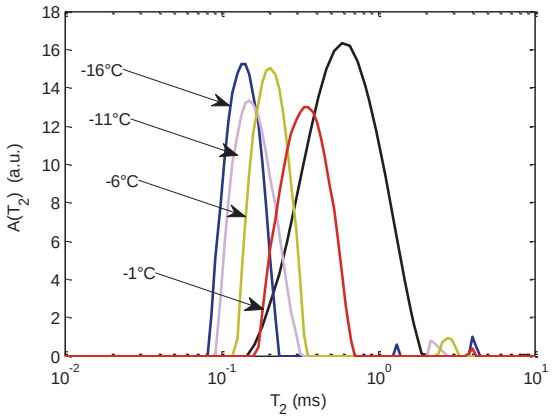

Figure 11: T_2 distribution obtained from relaxation measurements (black curve at 30°C) and at different temperature during melting.

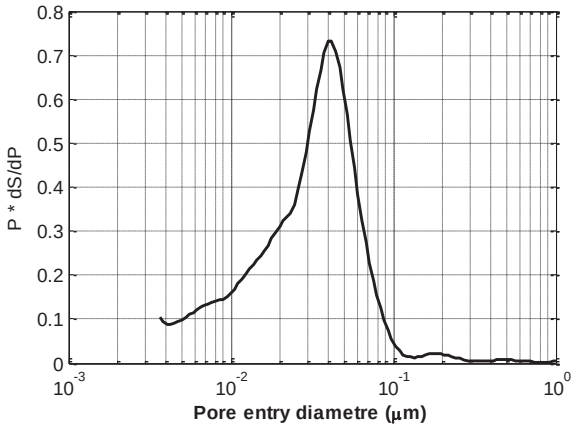

Figure 12: Pore size distribution obtained on the shale sample, high pressure mercury injection technique.

DISCUSSION

Pore size distribution deduced from NMR relaxation measurements relies on a diffusion process of molecules interacting with the pore surface yielding the well-known relationship with the surface to volume ratio. However, when molecules diffuse over distances that are larger, the surface to volume ratio is averaged over several pores. For standard reservoir samples in the mD or D permeability range, pore coupling is inherently present in many NMR relaxation measurement, especially at high temperature, but to a relatively small degree, except in certain cases. Hence, MICP measurements are often in agreement with NMR T_2 distributions and their direct comparison allows the calculation of an apparent surface relaxivity. Indeed, very often, the different pore size populations are grouped in well-defined regions of the porous media and therefore, the pore coupling is very limited. For example in carbonates, microporosity may be due to intra-grain porosity and these grains are large enough to avoid diffusive coupling. In shales, the pore sizes are roughly 2 or 3 orders of magnitude smaller. The permeability is then reduced to the nD range but this not the case for the diffusion coefficient. Indeed the latter primarily depends on porosity at first order. Indeed, from several measurements of diffusion in caprocks [10] and shales [11], we found that a reasonable estimation of the effective diffusivity can be made using an Archie relationship $D_{eff}/D_m = \Phi^{m-1}$ where D_m is the molecular diffusion coefficient of bulk water, with m varying between 1.8 and 2.5, as observed for electrical measurements. Hence, the diffusion coefficient decreases roughly linearly with porosity and the diffusion length $(6D_{eff}t)^{1/2}$ calculated at the peak relaxation time is still large. However, if the sample is heterogeneous at the micron scale (e.g. thin laminations or organic matter channels), one may find large T_2 distributions representing indeed the different pore populations. The correct interpretation of T_2 distributions in shales must be complemented by high resolution visualization of the pore network structure.

For the homogeneous shale sample studied here, the diffusion length at 0.7ms is about 1.4µm when taking a diffusion coefficient of 0.5×10^{-9} m^2/s,. Since we have a pore size distribution extending up to 100 nm, a strong coupling effect exist. Furthermore, in such case, a T_2-store-T_2 experiment cannot further demonstrate the coupling because an intermediate level of coupling is needed in such experiment (i.e. a bimodal or wide distribution is needed). Also, as suggested during the review of this manuscript, heterogeneous surface relaxivities within the porous media could also be a source of discrepancy when comparing different pore size distribution measurements. This effect would create larger T_2 relaxation distribution and to some degree compensate for the coupling effect. In the present situation the width of the distribution obtained by cryoporometry is about 2 decades, whereas it is about 1 decade or less for T_2 relaxation time distribution.

Interestingly, the pore entry size distribution obtained by high pressure mercury injection (HPMI) on a sister sample is relatively narrow with a peak at 40 nm, unlike the cryoporometry result (Figure 12). Although we often observe a correlation between pore size and pore throats, this correspondence is not necessarily true and is highly dependent

on the pore structure and geological history. At least, in terms of maximum size, the two distributions agree: the largest throat size is about 100 nm, while the largest pore size is about 300 nm (a ratio of 3 is the theoretical result for a sphere pack).

CONCLUSION

We show that pore size distribution obtained from NMR cryoporometry and relaxation experiments on the same sample can strongly disagree. While the cryoporometry technique is able to give accurate results from 2nm up to about 1µm, T_2 relaxation is strongly influenced by pore coupling. As a result, the distribution obtained from relaxation is representative on an average volume to surface ratio; in shales, this distribution also depends on the length scales of the heterogeneities present in the porous medium, compared to the diffusion length.

AKNOWLEDGEMENTS

We thank F. Norrant for providing the calibrated porous glasses, Elizabeth Rosenberg for performing the microCT images, and J. Labaume for the HPMI experiments.

REFERENCES

1 B. Lalanne, A. Le-Bihan, E. Elias, R. Poyol, L. Martinez, How to Cope with some of the Challenges Associated with Laboratory Measurements on Gas Shale Core Samples, in: Proceeding Soc. Pet. Eng. SPE 167709, 2014: pp. 1–17.

2 M. Fleury, E. Kohler, F. Norrant, S. Gautier, J. M'Hamdi, L. Barré, Characterization and Quantification of Water in Smectites with Low-Field NMR, J. Phys. Chem. C. 117 (2013) 4551–4560.

3 J. Strange, M. Rahman, E. Smith, Characterization of porous solids by NMR, Phys. Rev. Lett. 71 (1993) 3589–3591. doi:10.1103/PhysRevLett.71.3589.

4 O. V. Petrov, I. Furó, NMR cryoporometry: Principles, applications and potential, Prog. Nucl. Magn. Reson. Spectrosc. 54 (2009) 97–122. doi:10.1016/j.pnmrs.2008.06.001.

5. J. Mitchell, J. Webber, J. Strange, Nuclear magnetic resonance cryoporometry, Phys. Rep. 461 (2008) 1–36. doi:10.1016/j.physrep.2008.02.001.

6 J.B.W. Webber, Studies of nano-structured liquids in confined geometries and at surfaces, Prog. Nucl. Magn. Reson. Spectrosc. 56 (2010) 78–93. doi:10.1016/j.pnmrs.2009.09.001.

7 M. Fleury, J. Soualem, Quantitative analysis of diffusional pore coupling from T2-store-T2 NMR experiments., J. Colloid Interface Sci. 336 (2009) 250–9. doi:10.1016/j.jcis.2009.03.051.

8 P. Cosenza, J.C. Robinet, D. Prêt, E. Huret, M. Fleury, Y. Géraud, et al., Indirect estimation of the clay content of clay-rocks using acoustic measurements: New insights from the Montiers-sur-Saulx deep borehole (Meuse, France), Mar. Pet. Geol. (2013). doi:10.1016/j.marpetgeo.2013.07.004.

9 J.B.W. Webber, P. Corbett, K.T. Semple, U. Ogbonnaya, W.S. Teel, C. a. Masiello, et al., An NMR study of porous rock and biochar containing organic material,

Microporous Mesoporous Mater. 178 (2013) 94–98. doi:10.1016/j.micromeso.2013.04.004.
10 M. Fleury, S. Gautier, N. Gland, P. Boulin, B. Norden, C. Schmidt-Hattenberger, Advanced and integrated petrophysical characterization for CO2 storage: application to the Ketzin site., Oil Gas Sci. Technol. (2013).
11 M. Fleury, Characterization of shales withlow field NMR, in: Proceeding SCA Annu. Conf., 2014.

Table 1: Fraction in % of the different water populations from different methods (CPG sample).

Method	*15 nm*	*139nm*	*Inter-granular+bulk*
Weight	27.0	27.3	45.6
Cryoporometry	26.0	27.0	47.0
Relaxation	21.5	88.5	
Relaxation (-0.15°C)	28.4	24.6	-